ACS APPLIED MATERIALS & INTERFACES

Research Article

www.acsami.org

Intense Photoluminescence from Ceria-Based Nanoscale Lamellar Hybrid

Takaaki Taniguchi,*[,†,‡] Yuki Sonoda,[†] Makoto Echikawa,[†] Yusuke Watanabe,[†] Kazuto Hatakeyama,[†] Shintaro Ida,[§] Michio Koinuma,[†,‡] and Yasumichi Matsumoto[†,‡]

[†]Graduate School of Science and Technology, Kumamoto University, 2-39-1 Kurokami, Kumamoto 860-8555, Japan

[‡]JST, CREST, 5 Sanbancho, Chiyoda-ku, Tokyo 102-0075, Japan

[§]Department of Applied Chemistry, Faculty of Engineering, Kyusyu University, 744 Motooka, Nishi-ku, Fukuoka 819-0395, Japan

Supporting Information

ABSTRACT: Nanosheets, which are ultrathin inorganic crystals, have the potential to exhibit unique surface states and quantum effects. These nanosheets can be further manipulated to form lamellar structures for the fabrication of advanced hybrid nanomaterials. Here we report that conventionally nonluminescent ceria yields intense UV photoluminescence with an internal quantum yield (QY) of 59% when self-organized into a nanosheet lamellar architecture with dodecyl sulfate (DS) bilayers. The origin of luminescence exist at the organic/inorganic interfaces, where surface Ce^{3+} ions of ceria nanosheet layers graft with DS anions to activate radiative 5d→4f transition.

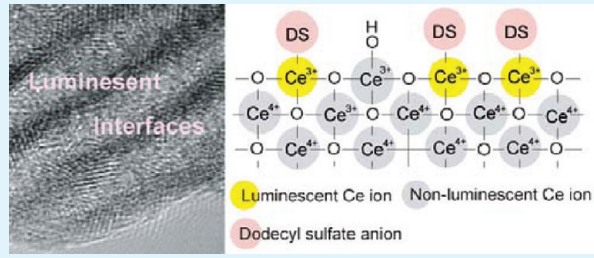

KEYWORDS: *nanosheets, ceria, hybrid, luminescence, synthesis, layard materials*

INTRODUCTION

For a decade, chemistry has contributed to the synthesis of nanomaterials with precisely controlled structures, chemical compositions and properties. Nanosheets (NSs) are promising next-generation nanomaterials. The two-dimensional anisotropy and nanoscale thickness provide two-dimensional quantum effects and unique surface bonding states, which potentially give rise to outstanding physical and chemical properties such as those discovered in graphene.[1] These promising features have motivated a number of extensive studies to synthesize and characterize novel NSs involving metals,[2] oxides,[3−6] hydroxides,[7,8] and sulfates.[9,10]

Furthermore, the nanoscale hybridization of inorganic NSs with ions, clusters, and molecules can offer dense integration of unique interface properties at the bulk scale.[11,12] For example, Sofos et al. have reported that 1 nm thick sheets of polycrystalline ZnO with interlayer organic dyes exhibit the highest photocurrent for organic, hybrid, and amorphous silicon by selective excitation of the dyes.[12] Our research group has synthesized titania nanosheet-based layered materials with lanthanide ions as guest species,[13,14] which allows to the high luminescent sensitivity depending on humidity as well as applied voltage. These studies have successfully employed layered structures to synergistically enhance the active properties of nanosheets and intercalated materials. It is also significant that the lamellar material could be synthesized using a nontoxic aqueous solution method with inexpensive metal salts, which realizes novel device fabrication that is cost-effective and eco-friendly.

Ceria (CeO_{2-x}) exhibits multifunctional properties involving high mechanical strength, oxygen ion conductivity, oxygen storage capacity, and strong UV absorption properties as well as photochemical activities, while doping of rare earth ions such as Eu^{3+}, Tb^{3+}, and Er^{3+} into ceria is investigated to yield well-defined luminescence.[15−17] To date, ceria nanostructures such as nanorods,[18,19] nanocubes,[20,21] and nanotubes[22] have been examined to tune the physical/chemical properties for the such applications. In the present study, we have investigated nanoscale lamellar hybrids based on ceria NSs. We discover that undoped ceria that is conventionally nonluminescent exhibits very intense UV photoluminescence at 380 nm with a high internal quantum yield (QY) of ca. 59% when self-organized into a nanosheet lamellar hybrid with dodecyl sulfate (DS) anions. Spectroscopic studies reveal that the ceria-DS layered hybrid yields efficient Ce^{3+} 4f→5d radiative transitions, where the luminescent pathway is quenched significantly in conventional ceria-related materials.

EXPERIMENTAL SECTION

Synthesis of Ceria NS-DS Hybrid. aqueous solutions of $Ce(NO_3)_3{\cdot}6H_2O$ (0.05 M, Wako, 99.5%), sodium dodecyl sulfate (SDS; 0.1M, Wako, 99.5%), and hexamethylenetetramine (HMT; 2 M Wako, 99.5%) were prepared with Milli-Q water. Twenty millilters of cerium nitrate solution was added to a mixed solution of 10 mL of SDS and 1 mL of HMT and 20 mL of water in a 50 cm^3 vessel. The

Received: November 27, 2011
Accepted: January 18, 2012
Published: January 18, 2012

mixed solutions were heated at 80 °C for 6 h. After the reaction, precipitates were obtained by centrifugation and washed with distilled water and ethanol, and then dried at room temperature (RT) under vacuum.

Synthesis of Reference Ceria NPs and Surface Modification with DS. Twenty milliliters of cerium nitrate solution was added to a mixed solution of 1 mL of HMT and 20 mL of water in a 50 cm^3 vessel. The mixed solutions were heated at 80 °C for 6 h. For the surface modification, products (ceria NPs) were dispersed in 0.1 M SDS aqueous solution under vigorous stirring for 1 day, and then collected by centrifugation and washed with distilled water and ethanol, and finally dried at room temperature (RT) under vacuum.

Exfoliation of Ceria NS-DS Hybrid into Unilamellar NSs. The dried product was dispersed in formamide (Wako, 99.5%) by ultrasonic treatment. A stable colloidal solution of exfoliated nanosheets was obtained after centrifugation at 3000 rpm for 20 min.

Characterizations. the crystal structures were analyzed from XRD (Rigaku RINT-2500VHF) patterns obtained using Cu Kα radiation (λ = 1.54056 Å). The thickness of the exfoliated nanosheets was confirmed by AFM (Veeco Nanoscope-V) measurements. PL spectra were obtained using a spectrofluorometer (Jasco FP-6500) with a 150 W Xe lamp at room temperature. The excitation and emission spectra were corrected for the spectral distribution of the Xe lamp intensity using rhodamine B (5.5 g/L, ethylene glycol solution) and a reference light source (Jasco ESC-333). The QY and UV−vis reflectance spectra were measured using a spectrofluorometer with an integrating sphere (Jasco ILF-533). The internal quantum yield (QY_{int}) can be obtained by the following equation.

$$QY_{int} = N_{em}/(N_{inc} - N_{ref})$$

Where N_{em} is number of photons emitted by the sample, N_{inc} is number of photons irradiated on the sample, N_{ref} is number of photons reflected by the sample and the standard.

The accuracy of the QY measurements was confirmed by measurement of a standard quinine sulfate solution. The incident/detection wavelengths for UV−vis reflection spectroscopy were controlled to be the same. Luminescent decay time was measured using a Hamamatsu Quantaurus-tau measurement system. The sample was excited on 280 nm for the measurements. XPS measurements were performed in a vacuum less than 1×10^{-7} Pa using a spectrometer (Thermo Scientific Sigma Probe) equipped with a monochromatized X-ray source (1486.6 eV). Electrons emitted from the samples were detected by a hemispherical energy analyzer equipped with six channeltrons. The overall energy resolution for XPS was below 0.55 eV (on Ag $3d_{3/2}$ with a pass energy of 15 eV). The XPS peaks were deconvoluted using Gaussian components after Shirley background subtraction. Raman spectroscopy was performed using a micro-Raman spectrometer (Jasco NRS-3100) with a 532 nm excitation source at room temperature. Field-emission scanning electron microscopy (SEM; Hitachi, SU-8000) was performed in secondary electron imaging mode with an acceleration voltage of 5 kV. The room temperature infrared (IR) Fourier-transform spectra were recorded on a Jeol JIR-7000 spectrometer. The products (20 mg) were thoroughly ground with (400 mg) potassium bromide powder (KBr for IR, Wako), and subjected to IR analysis.

RESULTS AND DISCUSSION

We have synthesized lamellar hybrids based on ceria nanosheets for the first time by a simple aqueous solution route. In a typical synthesis, $Ce(NO_3)_3$ solution is added into a mixed solution of hexamethylenetetramine (HMT) and sodium dodecyl sulfate (SDS) with a molar ratio of Ce/DS of 1, and subsequently heated at 80 °C for 6 h. Synthesis generally yields submicrometer thickness plates that are several micrometers wide (see the Supporting Information, Figure S1). X-ray diffraction (XRD) patterns (Figure 1a) of the lamellar product have sharp (00*l*) basal reflections labeled with asterisks in the low angular region (up to 35°), which indicates a highly

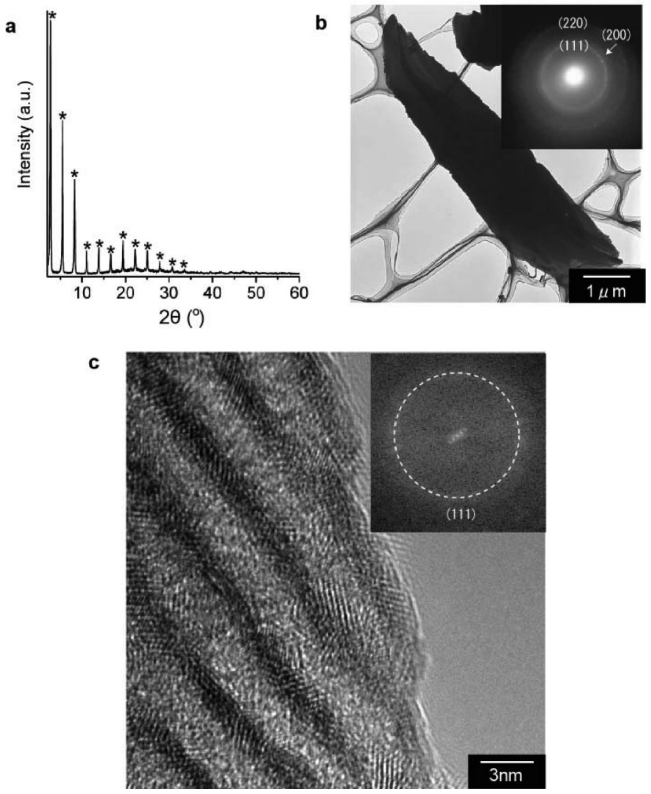

Figure 1. (a) XRD pattern of ceria NS-DS hybrid; asterisk indicate (00*l*) reflections from a lamellar structure. (b) Low-magnification TEM image and ED pattern. (c) Cross-sectional HRTEM image; an inserted fast-Fourier transform (FFT) image presents a ring pattern that can be indexed in the cubic fluorite CeO_2 phase (JCPDS #34−0394).

developed lamellar structure with the basal spacing of 3.2 nm calculated with Bragg's equation using the theta value of (001) reflection. No remarkable reflections from known cerium-containing oxide, hydroxide, or carbonate phases were observed over the entire range measured, which suggests an extremely thin Ce-based inorganic layer.

A selected electron diffraction pattern (SAED) of the lamellar structure gives a distinct ring pattern that can be indexed in the ceria phase (Figure 1b) (JCPDS #34−0394), which suggests that the ceria layers are polycrystalline throughout the entire lamellar architecture. High-resolution transmission electron microscopy (HRTEM) (Figure 1c) confirms that the lamellar structure is composed of alternating layers of approximately 1.5 nm thick ceria layers (dark) and 2 nm thick DS bilayers (bright). The 1.5 nm ceria layer is approximately three times that of the CeO_2 lattice constant (0.54 nm), while consideration of the DS molecular length (ca. 1.9 nm) suggest that the 2 nm thick DS bilayer consists of DS anions tilted with respect to the nanosheet surface. Careful observation reveals that the individual nanosheet layer contains two-dimensionally connected nanosized grains with no preferential orientation (also see Figure 5b), which accords well with the SAED study. The formation mechanism of polycrystalline ceria layers is described as follows. Although trivalent rare earth (Re) ions generally favor Re(III)-hydroxide formation in a reaction with a base solution, $Ce(OH)_3$ is known to be unstable under the given reaction conditions, so that ceria (oxide) is produced with partial oxidation and dehydration of cerous hydroxides.[22] In fact, ceria nanoparticles (10 nm in an

average size) were formed when the synthesis was performed without the SDS additive (see the Supporting Information, Figure S2). On these bases, single-crystal-like $Ce(OH)_3$ layers are likely formed between DS bilayers during the initial growth stage, and then ceria nanocrystals are nontopotactically nucleated in the hydroxide matrix. The proposed mechanism is similar to that for the formation of ZnO lamellar, where a $Zn(OH)_2$ nanosheet layer with preferential crystallographic orientation is nontopotactically converted to a two-dimensional ZnO nanosized grain network when annealed at 150 °C in air.[12] Note that optimization of the reaction conditions was crucial for the successful formation of the ceria-DS lamellar structure. If the reaction temperature was increased to be 120 °C, or amount of SDS was decreased to adjust the molar ratio of Ce/DS to be 2 in a starting solution, ceria nanoparticles were predominantly formed (see the Supporting Information, Figure S2).

Further structural information was provided by Raman and IR spectroscopy. The Raman spectrum (Figure 2a) shows a strong band at 464 cm^{-1} that corresponds to a triply degenerate Raman-active phonon of the cubic CeO_2 fluorite phase with the space group $Fm3m$,[23] which supports that the inorganic layer is based on the ceria phase rather than other cerium-based compounds. The DS layers in the lamellar structure provide the other Raman bands. In particular, strong bands detected in 1000−1200 cm^{-1} region correspond to symmetric OSO_3 vibration,[24] of which the peak positions are close to those from SDS, while the relative peak-intensities in each spectrum are significantly different, suggesting a unique geometry of DS anions between ceria layers. In the IR spectra of ceria NS-DS hybrid and SDS powder (Figure 2b), a series of bands in the 2750−3000 cm^{-1} region are attributable to the symmetric and asymmetric stretching of the CH_2 groups and the terminal CH_3 group. The bands around 3400 cm^{-1} are attributed to the O−H stretching. From 1100 to 1350 cm^{-1}, the spectrum exhibits asymmetric stretching bands of OSO_3 group.[25] In this region, SDS powder gives a main band at 1220 cm^{-1}, whereas the band appears at 1175 cm^{-1} for the ceria NS-DS hybrid. The vibration mode corresponding to the band is parallel to the DS anion and therefore is sensitive to direct contact with surfaces.[24] According to the literature,[26] adsorption of DS anion on various metal oxides (TiO_2, ZrO_2 Al_2O_3, and Ta_2O_5) slightly shifts the band position within 10 cm^{-1} via electrostatic interactions through the surface hydroxyl groups. In the present case, the shift in the band position is remarkably large (45 cm^{-1}), which suggests that SO_3^- moiety directly coordinates with the Ce ions at the ceria nanosheet surfaces.

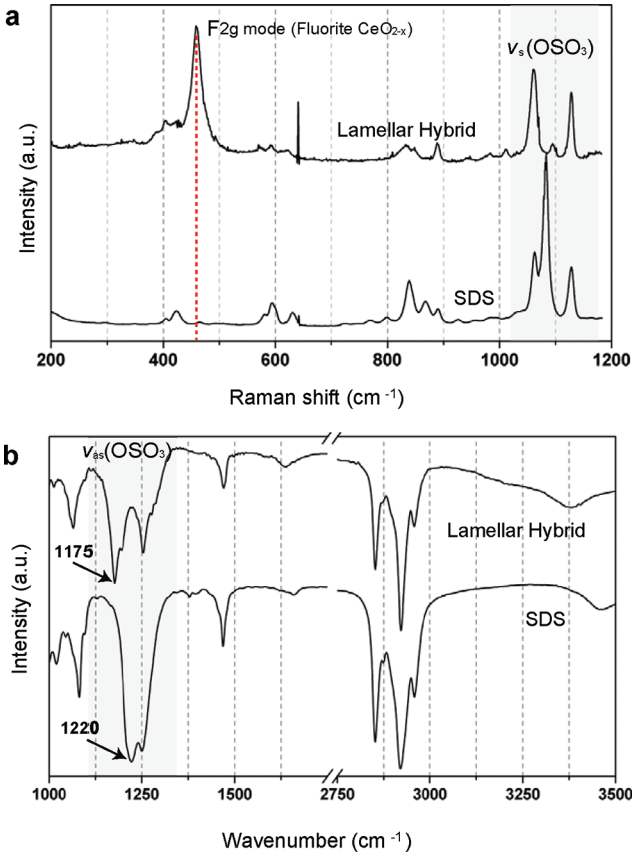

Figure 2. Raman and IR spectra for ceria lamellar NS-DS hybrid and SDS powder.

Although undoped ceria can show photoluminescence given by hopping from defect levels to the O2p band,[27−30] such defect-mediated luminescence is weak in general because of nonradiative pathways induced simultaneously by defects. However, surprisingly, undoped ceria NS-DS layered hybrid displayed violet luminescence clearly visible to naked eyes upon UV light irradiation (254 nm) with Hg lamp, while no luminescence was observed for SDS powders as well as reference 10 nm-size ceria nanoparticles (NPs) synthesized without SDS. Therefore, in the present case, individually nonluminescent ceria and DS anions are self-organized in a nanoscale lamellar architecture to produce luminescent functionality, which can be described as "self-functionalization". The photoluminescence (PL) emission spectra (Figure 3) demonstrate that the luminescence is decomposed in two bands at 373 and 396 nm with full-width at half maxima (fwhm) of approximately 25 and 45 nm, respectively. The double-peak luminescence suggests direct emission from the ^2D ($5d^1$) state of Ce^{3+} to the two split $4f^1$ ground states of $^2F_{5/2}$ and $^2F_{7/2}$ caused by spin−orbit coupling,[31] while the excitation spectrum monitored at 380 nm emission (Figure 3) shows a band around 284 nm attributable to the Ce^{3+} 4f→5d transition.

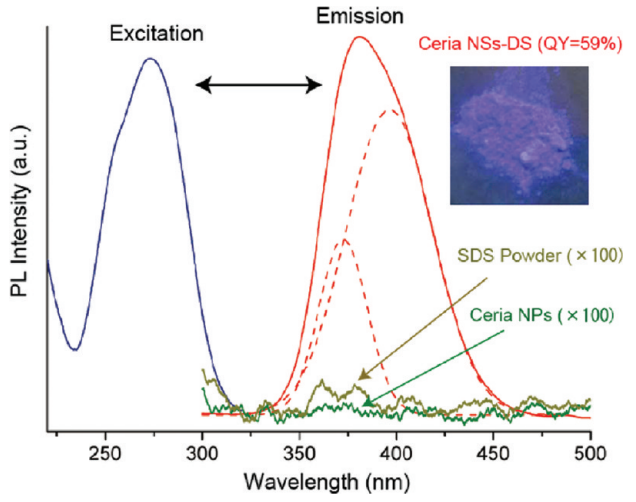

Figure 3. PL emission spectra (excited at 280 nm) and excitation spectra (monitored at 380 nm) for ceria NS-DS hybrid, reference ceria NPs, and SDS powder.

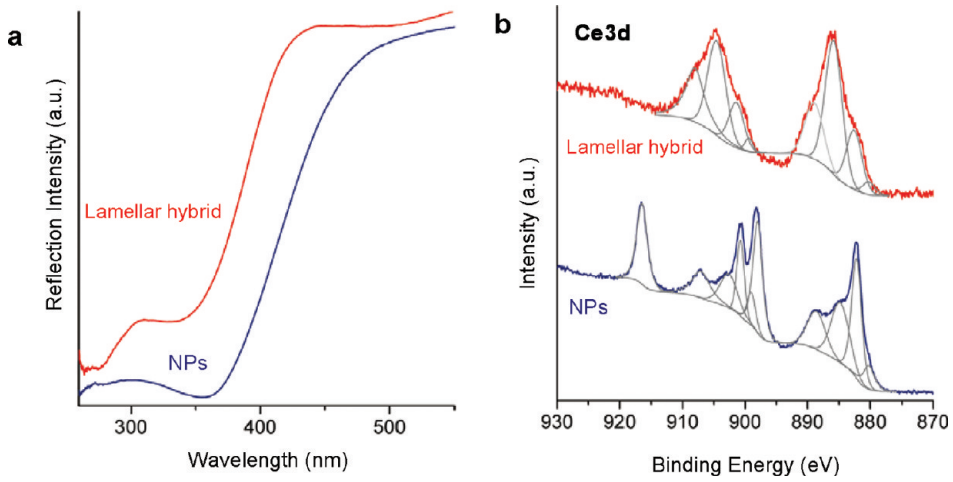

Figure 4. (a) UV−vis reflection and (b) Ce3d XP spectra for ceria NS-DS hybrid and reference ceria NPs.

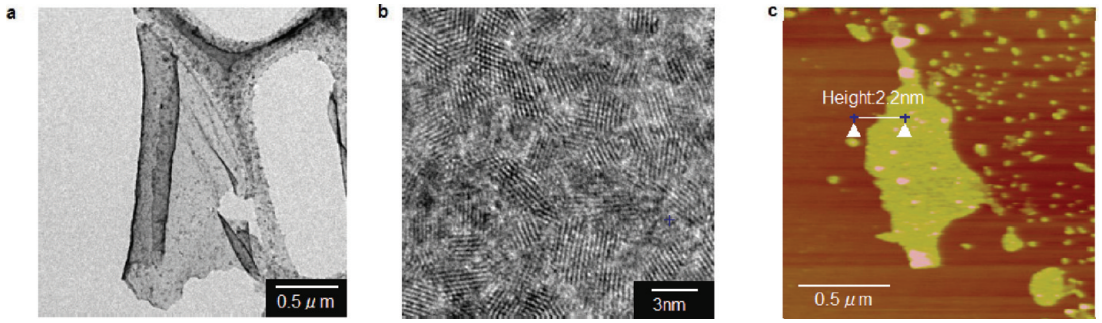

Figure 5. (a) Low-magnification image of an exfoliated nanosheet. (b) HRTEM image of a part of the nanosheet. (c) AFM image of exfoliated nanosheets.

The lamellar hybrid offers a very high QY (59%) of UV luminescence upon excitation at 280 nm. The decay constant of this band was measured to be approximately 50 ns (Supporting Information, Figure S3). This value is comparable to those previously reported for Ce^{3+}-activated phosphors,[32,33] which evidenced that the Ce^{3+} ion is responsible for the UV emission band.

UV−vis diffuse reflectance spectroscopy was performed to further elucidate the emission mechanism for the lamellar hybrid (Figure 4a). Both the ceria NS-DS hybrid and reference NPs show strong absorption in the UV region from an $O^{2-} \rightarrow Ce^{4+}$ charge transfer (CT) transition.[34] Lamellar hybrid exhibits an enhanced absorption band at ca. 270 nm due to the 4f→5d absorption, in addition to the CT band. The $O^{2-} \rightarrow Ce^{4+}$ CT band does not overlap with the PL excitation spectra for the ceria NS-DS hybrid; therefore, this excitation process is not involved in the luminescent mechanism.

XPS data (Figure 4b) shows that the ceria NS-DS hybrid involves remarkably high concentration of Ce^{3+}. The $Ce^{3+}/(Ce^{4+} + Ce^{3+})$ atomic ratio, calculated from the peak areas using the deconvolution procedure,[35] corresponded to 0.48 and 0.28 for the lamellar hybrid and reference ceria NPs, respectively. Although the XPS analysis might overestimate the Ce^{3+} concentration due to the reduction of Ce^{4+} to Ce^{3+} during measurements preformed under high-vacuum conditions,[36] it is commonly accepted that the ceria surface strongly favors Ce^{3+} formation,[37] and therefore, the higher $Ce^{3+}/(Ce^{4+} + Ce^{3+})$ atomic ratio of ceria NSs than ceria NPs should be given by the significantly high surface to volume ratio due to the extremely thin thickness of NSs. It is notable that, according to the XPS and TEM-EELS investigations, ceria nanoparticles with tiny sizes can show such high or even higher concentrations of Ce^{3+} spices while keeping the fluorite phase;[38,39] however, 5d→4f (Ce^{3+}) luminescence form those nanoparticles are quenched, as the Ce^{3+} ions at nanoparticle surfaces strongly favor bonding with OH groups, which is a very effective quenching ligand because of its large vibrational energy. On the other hand, surface Ce^{3+} ions of ceria nanosheets in the lamellar structure were passivated by sulfonate-moiety, as indicated by IR analysis, and the number of nonradiative pathways due to the OH groups should be reduced significantly. It is worth mentioning that the 5d orbitals of Ce^{3+} ions are sensitive to the ligand sphere, so that many organic ligands have been found to quench Ce^{3+} luminescence upon complexation; organic ligands that effectively activate Ce^{3+} luminescence remain rather rare, for example, diazapolyoxabicyclic ligands (cryptands) and polybenzimidazole tripodal ligands allow radiative 5d→4f transitions.[32,40] Therefore, DS anion could play a crucial role to give luminescent functionality in addition to the formation of the layered structure. It is also notable that Ce^{3+} 4f→5d radiative transitions were not detected for the referenced ceria NPs even after surface-modification with DS anion by mixing these NPs and SDS aqueous solution, whereas IR analysis confirmed that the sample involved DS (see the Supporting Information, Figure S4), indicating that the nanoscale layered structure is greatly contributed to luminescent properties. So far, we have proposed that the formation of dense integration of interfacial Ce^{3+}-sulfonate centers in the lamellar structure could give excellent luminescent properties to the ceria NS-DS hybrid.

dx.doi.org/10.1021/am201613z | ACS Appl. Mater. Interfaces 2012, 4, 1010−1015

We also investigated in the exfoliation of the lamellar structure into unilamellar nanosheets, which are highly attractive as building blocks for the fabrication of nanostructured devices. TEM observation (Figure 5a) showed that the presence of nanosheets, and HRTEM image (Figure 5b) of a part of the unilamellar nanosheet demonstrated that they are composed of ceria nanocrystals connected two-dimensionally. The atomic force microscopy (AFM) image (Figure 5c) shows that the nanosheet thickness was ca. 2 nm, which is much thinner than the basal spacing determined from XRD data (3.2 nm) and is rather close to the thickness of the ceria layer observed by HRTEM (1.5 nm), which indicated that DS anions were removed from the ceria surface during the exfoliation process. Along with the products well-defined sheetlike morphology, small ones (size less than 100 nm) are also observed, though their thickness is uniform (ca. 2 nm). This observation indicates that the ceria layers were not robust due to the polycrystalline nature so that they were broken partially by the exfoliation process. We note that the photoluminescence was quenched drastically by the exfoliation process (see the Supporting Information, Figure S5), which can be interpreted that replacement of DS^- with OH^- and/or formamide upon the exfoliation quenched the luminescence.

Traditionally, rare earth activated phosphors have been explored based on inorganic materials such as metal fluoride, oxides, sulfates, and nitrides or complexes,[41] whereas in the present study, we could have established inorganic/organic layered phosphors with interfacial luminescent centers where the luminescent properties could be, in principle, controlled by appropriate selection of the nanosheet and organic layers. Such novel phosphors may further develop luminous sources for lasers, displays, and fluorescent lamps. In particular, ceria-based lamellar hybrid phosphors are potentially applicable in sensors, because of the redox properties based on reversible oxidation/reduction of $Ce^{4+} \Leftrightarrow Ce^{3+}$ in the fluorite phase.[42,43]

CONCLUSION

In summary, we succeed in the synthesis of ceria NS-DS layered materials and the exfoliation into unilamellar nanosheets. We discovered that conventionally nonluminescent ceria exhibit intense UV photoluminescence at 380 nm when self-organized into a nanosheet lamellar hybrid with DS anions. Microscopic studies show a well-developed lamellar structure with alternate stacking of approximately 1.5 nm thick polycrystalline ceria layers and 2 nm thick DS bilayers. Spectroscopic studies suggest that DS anion coordinates with Ce^{3+} ions on the ceria NS surface, which results in the activation of radiative 5d →4f transitions, whereas the transition is not allowed for conventional ceria nanoparticles, due to the surface hydroxyl groups. Therefore, it can be concluded that DS anion plays a double role to form the layered structure, and to provide luminescent functionality. Our results develop a concept for material design; namely, nanosheet-organic lamellar hybrids can provide a novel functionality that is inactive for both individual inorganic and organic components.

ASSOCIATED CONTENT

Supporting Information

SEM images of ceria NS-DS lamellar hybrid (Figure S1). XRD patterns of reference ceria NPs synthesized by the reaction of $Ce(NO)_3$ with HMT solutions at 80 °C for without SDS additive (molar ratio of Ce/DS = 1), ceria NPs synthesized at 80 °C with SDS additive (molar ratio of Ce/DS = 2), and ceria NPs synthesized at 120 °C with SDS additive (molar ratio of Ce/DS = 1) (Figure S2). PL luminescent decay time of 380 nm-luminesce excited at 280 nm (Figure S3). IR spectra of ceria NPs modified by DS (Figure S4). Emission and excitation of a colloidal solution of exfoliated ceria NSs in formamide (Figure S5). This material is available free of charge via the Internet at http://pubs.acs.org.

AUTHOR INFORMATION

Corresponding Author

*Phone: +81- (96)-342-3659. E-mail: takatani@gpo.kumamoto-u.ac.jp.

Notes

The authors declare no competing financial interest.

ACKNOWLEDGMENTS

This work was supported by the Core Research of Evolutional Science & Technology (CREST) of the Japan Science and Technology Agency, Grant-in-Aid for Young Scientists(B) (No. 23710131), and Grant-in-Aid for Scientific Research(A) (No. 23245036). The authors thank H. Tokimori (Tokyo Institute of Technology) for discussions regarding the TEM results; Y. Tanaka, A. Shigeta, Y. Matsuda, and Prof. C. Iwamoto (Kumamoto University) for performing TEM observations; and Y. Nojiri and A. Funatsu for the luminescence quantum yield and decay time measurements.

REFERENCES

(1) Novoselov, K. S.; Geim, A. K.; Morozov, S. V.; Jiang, D.; Katsnelson, M. I.; Grigorieva, I. V.; Dubonos, S. V.; Firsov, A. A. *Nature* **2005**, *438*, 197−200.
(2) Huang, X.; Tang, S.; Mu, X.; Dai, Y.; Chen, G.; Zhou, Z.; Ruan, F.; Yang, Z.; Zheng, N. *Nat. Nanotechnol.* **2011**, *6*, 28−32.
(3) Fukuda, K.; Ebina, Y.; Shibata, T.; Aizawa, T.; Nakai, I.; Sasaki, T. *J. Am. Chem. Soc.* **2007**, *129*, 202−209.
(4) Ida, S.; Ogata, C.; Eguchi, M.; Youngblood, W. J.; Mallouk, T. E.; Matsumoto, Y. *J. Am. Chem. Soc.* **2008**, *130*, 7052−7059.
(5) Omomo, Y.; Sasaki, T.; Wang, L.; Watanabe, M. *J. Am. Chem. Soc.* **2003**, *125*, 3568−3575.
(6) Choi, M.; Na, K.; Kim, J.; Sakamoto, Y.; Terasaki, O.; Ryoo, R. *Nature* **2009**, *461*, 246−249.
(7) Ida, S.; Shiga, D.; Koinuma, M.; Matsumoto, Y. *J. Am. Chem. Soc.* **2008**, *130*, 14038−14039.
(8) Ma, R.; Liu, Z.; Takada, K.; Iyi, N.; Bando, Y.; Sasaki, T. *J. Am. Chem. Soc.* **2007**, *129*, 5257−5263.
(9) Coleman, J. N.; Lotya, M.; O'Neill, A.; Bergin, S. D.; King, P. J.; Khan, U.; Young, K.; Gaucher, A.; De, S.; Smith, R. J.; Shvets, I. V.; Arora, S. K.; Stanton, G.; Kim, H. Y.; Lee, K.; Kim, G. T.; Duesberg, G. S.; Hallam, T.; Boland, J. J.; Wang, J. J.; Donegan, J. F.; Grunlan, J. C.; Moriarty, G.; Shmeliov, A.; Nicholls, R. J.; Perkins, J. M.; Grieveson, E. M.; Theuwissen, K.; McComb, D. W.; Nellist, P. D.; Nicolosi, V. *Science* **2011**, *331*, 568−571.
(10) Schliehe, C.; Juarez, B. H.; Pelletier, M.; Jander, S.; Greshnykh, D.; Nagel, M.; Meyer, A.; Foerster, S.; Kornowski, A.; Klinke, C.; Weller, H. *Science* **2010**, *329*, 550−553.
(11) Yamamoto, T.; Saso, N.; Umemura, Y.; Einaga, Y. *J. Am. Chem. Soc.* **2009**, *131*, 13196−13197.
(12) Sofos, M.; Goldberger, J.; Stone, D. A.; Allen, J. E.; Ma, Q.; Herman, D. J.; Tsai, W. W.; Lauhon, L. J.; Stupp, S. I. *Nat. Mater.* **2009**, *8*, 68−75.
(13) Ida, S.; Ogata, C.; Shiga, D.; Izawa, K.; Ikeue, K.; Matsumoto, Y. *Angew. Chem., Int. Ed.* **2008**, *47*, 2480−2483.
(14) Ida, S.; Unal, U.; Izawa, K.; Altuntasoglu, O.; Ogata, C.; Inoue, T.; Shimogawa, K.; Matsumoto, Y. *J. Phys. Chem. B* **2006**, *110*, 23881−23887.

(15) Babu, S.; Cho, J. H.; Dowding, J. M.; Heckert, E.; Komanski, C.; Das, S.; Colon, J.; Baker, C. H.; Bass, M.; Self, W. T.; Seal, S. *Chem. Commun.* **2010**, *46*, 6915−6917.
(16) Kumar, A.; Babu, S.; Karakoti, A. S.; Schulte, A.; Seal, S. *Langmuir* **2009**, *25*, 10998−11007.
(17) Dutta, D. P.; Manoj, N.; Tyagi, A. K. *J. Lumin.* **2011**, *131*, 1807−1812.
(18) Lu, X.; Zheng, D.; Zhang, P.; Liang, C.; Liu, P.; Tong, Y. *Chem. Commun.* **2010**, *46*, 7721−7723.
(19) Lu, X.; Zhai, T.; Cui, H.; Shi, J.; Xie, S.; Huang, Y.; Liang, C.; Tong, Y. *J Mater. Chem.* **2011**, *21*, 5569−5572.
(20) Taniguchi, T.; Katsumata, K. I.; Omata, S.; Okada, K.; Matsushita, N. *Cryst. Growth Des.* **2011**, *11*, 3754−3760.
(21) Yang, S.; Gao, L. *J. Am. Chem. Soc.* **2006**, *128*, 9330−9331.
(22) Tang, C.; Bando, Y.; Liu, B.; Golberg, D. *Adva. Mater.* **2005**, *17*, 3005−3009.
(23) Taniguchi, T.; Watanabe, T.; Sugiyama, N.; Subramani, A. K.; Wagata, H.; Matsushita, N.; Yoshimura, M. *J. Phys. Chem. C* **2009**, *113*, 19789−19793.
(24) Gao, X.; Chorover, J. *J. Colloid Interface Sci.* **2010**, *348*, 167−176.
(25) Zhang, X.; Yin, H.; Cheng, X.; Hu, H.; Yu, Q.; Wang, A. *Mater. Res. Bull.* **2006**, *41*, 2041−2048.
(26) Dobson, K. D.; Roddick-Lanzilotta, A. D.; McQuillan, A. J. *Vib. Spectrosc.* **2000**, *24*, 287−295.
(27) Lu, X. H.; Huang, X.; Xie, S. L.; Zheng, D. Z.; Liu, Z. Q.; Liang, C. L.; Tong, Y. X. *Langmuir* **2010**, *26*, 7569−7573.
(28) Mochizuki, S.; Fujishiro, F. *Phys. Status Solidi B* **2009**, *246*, 2320−2328.
(29) Gao, F.; Li, G. H.; Zhang, J. H.; Qin, F. G.; Yao, Z. Y.; Liu, Z. K.; Wang, Z. G.; Lin, L. Y. *Chin. Phys. Lett.* **2001**, *18*, 443−448.
(30) Choi, W. C.; Lee Nyung, H.; Kim, Y.; Park, H. M.; Kim, E. K. *Jpn. J. Appl. Phys.* **1999**, *38*, 6392−6393.
(31) Aull, B. F.; Jenssen, H. P. *Phys. Rev. B: Condens. Matter Mater. Phys.* **1986**, *34*, 6647−6655.
(32) Zheng, X. L.; Liu, Y.; Pan, M.; Lü, X. Q.; Zhang, J. Y.; Zhao, C. Y.; Tong, Y. X.; Su, C. Y. *Angew. Chem., Int. Ed.* **2007**, *46*, 7399−7403.
(33) Aull, B. F.; Jenssen, H. P. *Phys. Rev. B: Condens. Matter Mater. Phys.* **1986**, *34*, 6640−6646.
(34) Tsunekawa, S.; Fukuda, T.; Kasuya, A. *J. Appl. Phys.* **2000**, *87*, 1318−1321.
(35) Burroughs, P.; Hamnett, A.; Orchard, A. F.; Thornton, G. *J. Chem. Soc. Dalton* **1976**, 1686−1698.
(36) Zhang, F.; Wang, P.; Koberstein, J.; Khalid, S.; Chan, S. W. *Surf. Sci.* **2004**, *563*, 74−82.
(37) Tsunekawa, S.; Ishikawa, K.; Li, Z. Q.; Kawazoe, Y.; Kasuya, A. *Phys. Rev. Lett.* **2000**, *85*, 3440−3443.
(38) Wu, L.; Wiesmann, H. J.; Moodenbaugh, A. R.; Klie, R. F.; Zhu, Y.; Welch, D. O.; Suenaga, M. *Phys. Rev. B: Condens. Matter Mater. Phys* **2004**, *69*, 1254151−1254159.
(39) Tsunekawa, S.; Fukuda, T.; Kasuya, A. *Surf. Sci.* **2000**, *457*, 437−440.
(40) Blasse, G.; Dirksen, G. J.; Sabbatini, N.; Perathoner, S. *Inorg. Chim. Acta* **1987**, *133*, 167−173.
(41) Binnemans, K. *Chem. Rev.* **2009**, *109*, 4283−4374.
(42) Karakoti, A. S.; Monteiro-Riviere, N. A.; Aggarwal, R.; Davis, J. P.; Narayan, R. J.; Seif, W. T.; McGinnis, J.; Seal, S. *JOM* **2008**, *60*, 33−37.
(43) Trovarelli, A. *Catal. Rev.* **1996**, *38*, 439−520.